Ocean Sci. Discuss., 11, 839–893, 2014
www.ocean-sci-discuss.net/11/839/2014/
doi:10.5194/osd-11-839-2014

Ocean Science
Discussions
Open Access

Sensitivity of phytoplankton distributions to vertical mixing along a North Atlantic transect

L. Hahn-Woernle[1], H. A. Dijkstra[1], and H. J. Van der Woerd[2]

[1]Institute for Marine and Atmospheric Research Utrecht (IMAU), Dept. of Physics and Astronomy, Utrecht University, P.O. Box 80.005, 3508 TA Utrecht, the Netherlands
[2]Institute for Environmental Studies (IVM), Free University of Amsterdam, the Netherlands

Received: 31 January 2014 – Accepted: 20 February 2014 – Published: 14 March 2014

Correspondence to: L. Hahn-Woernle (l.hahn-woernle@uu.nl)

Published by Copernicus Publications on behalf of the European Geosciences Union.

Abstract

Using in situ data of upper ocean vertical mixing profiles along a transect in the North Atlantic and an idealised phytoplankton growth model (PGM), we study the sensitivity of the surface phytoplankton concentration to vertical mixing distributions. Optical parameters in the PGM are calibrated with observations of light attenuation. The calibration of the biological parameters in the PGM is carried out at three different referent stations with observed vertical profiles of chlorophyll *a* (Chl *a*) and nutrient concentration. Vertical mixing profiles at all other stations are next used at the reference stations to study the sensitivity of modelled phytoplankton distributions to vertical mixing. We find that shifts in vertical mixing are able to induce a transition from an upper chlorophyll maximum to a deep one and vice-versa. Furthermore, a clear correlation between the surface phytoplankton concentration and the mixing induced nutrient flux is found in nutrient limited regions. This may open up the possibility to extract characteristics of vertical mixing from satellite ocean colour data using data-assimilation methods.

1 Introduction

Thanks to the long-term in situ and satellite observations, the study of the plankton variability on time scales longer than seasonal has come within reach. On interannual-to-decadal time scales, changes in chlorophyll *a* (Chl *a*) concentrations can be well correlated (Martinez et al., 2009) to variations in climate indices such as the North Atlantic Oscillation. Based on a century long database of in situ Chl *a* and ocean transparency measurements, long-term trends in Chl *a* were presented in Boyce et al. (2010). Although the results are under debate, it is clear that long-term trends in Chl *a* are non-uniform over the globe and well correlated to the increase in sea surface temperature (SST). For the North Atlantic (north of 20° N), Wernand et al. (2013) found an average rate of increase of about 0.0071 mg $(m^3\,yr)^{-1}$ over the last century. On a shorter time

OSD
11, 839–893, 2014

scale (decades), however, much larger local variations are observed (Antoine et al., 2005).

Although the precise details of a phytoplankton bloom are still not clarified, most of the theories consider vertical mixing as a key factor in its onset (Behrenfeld et al., 2006). During winter, deep mixing brings nutrients into the euphotic layer but light is limited. In spring, the shallowing of the mixed layer allows the phytoplankton to spend more time exposed to light. The latter enhances growth and leads to an upper chlorophyll maximum (UCM) when enough nutrients are available (Behrenfeld, 2010; Lozier et al., 2011). Since photosynthetically active radiation (PAR) is absorbed at the surface, less radiation penetrates the water column, which has a strong impact on the growth below the mixed layer. As soon as the necessary nutrients (e.g. phosphorus and nitrogen) are depleted, the phytoplankton concentration in the mixed layer decreases giving the phytoplankton below the mixed layer the possibility to grow. In this case most of the phytoplankton cells are found below the mixed layer forming a so-called deep chlorophyll maximum (DCM). A DCM is the most dominant appearance of phytoplankton in strongly stratified regions such as the sub-tropical North Atlantic.

Qualitative mechanisms aiming to explain the relation between SST and Chl *a* concentrations have, for example, been suggested by Doney (2006). In areas where phytoplankton is nutrient limited, e.g. in the mid-latitude Atlantic, an increase in SST will inhibit vertical mixing and lead to stratification. In a warming ocean the transport of nutrients into the upper ocean is hence expected to decrease. In areas where the phytoplankton is light limited, such as in the northern North Atlantic, an SST increase will reduce the depth of the mixed layer and hence one would expect an increase in phytoplankton. The fact that this trend is not observed in high-latitude regions according to data in Boyce et al. (2010) indicates that vertical mixing processes are not solely controlled by the background stratification. Indeed, it is known from basic upper-ocean turbulence measurements and theory that, apart from the surface buoyancy forcing, vertical mixing is also strongly dependent on the surface wind-stress forcing. In addition, the background stratification can also be substantially affected by advection of

OSD
11, 839–893, 2014

heat and salt due to ocean currents, and in particular by the presence of meso-scale eddies (McGillicuddy et al., 2007).

At any particular location in the open ocean, the vertical profile of the mixing coefficient K_T [$m^2 s^{-1}$] (for heat and salt) is determined by the background stratification (or buoyancy frequency N), the turbulent kinetic energy dissipation rate ε [$m^2 s^{-3}$] and a mixing efficiency (Jurado et al., 2012b). Over the last decade, microstructure turbulence measurements of the upper ocean have been carried out along a few sections in the Atlantic Ocean, see Roget et al. (2006) for an overview. Using a microstructure profiler, the distribution of K_T along a south to north transect in the eastern North Atlantic during the STRATIPHYT-I cruise in July–August 2009 and the STRATIPHYT-II cruise in April–May 2011 was determined (Jurado et al., 2012b, a). Satellite ocean colour observations (MODIS-AQUA) of August 2009 indicate a meridional gradient in Chl *a* at this time of the year. The profiles of K_T along this section clearly indicate high values in the upper mixed layer and a decrease near the base of the mixed layer. At some locations the averaged station profiles of K_T slightly increase below the mixed layer before background values of 10^{-5}–10^{-4} $m^2 s^{-1}$ are approached at about 100 m depth. In spring 2011 satellite ocean colour observations are characterised by a high concentration around 45° N and decreasing Chl *a* concentrations north and south of this. In situ vertical mixing profiles of K_T indicate that the water column is stratified up to about this latitude. Further north the water column is more homogeneously mixed down to 100 m depth (Jurado et al., 2012b, a).

The effect of vertical mixing on phytoplankton distributions can be studied using ocean-phytoplankton models. These models, however, contain a number of uncertain parameters both in the turbulence model and in the plankton model. Usually, the parameter values are "tuned" to observations at one particular well-observed location and the response of the model at other locations to a different surface forcing can then be studied under the assumption that these parameters do not change (Omta et al., 2009). In very special circumstances, a vertical profile of the mixing coefficient K_T is available for verification of the quality of the turbulence model used (Johnk et al., 2008).

OSD
11, 839–893, 2014

This work is motivated by the availability of an observed integral picture (forcing, mixing, nutrients, phytoplankton, optical properties) over the eastern Atlantic transect during Summer 2009 and Spring 2011 from the STRATIPHYT cruises. Using ocean-plankton models and data-assimilation methods we eventually aim to tackle an ambitious inverse problem: provided satellite derived ocean colour data and the meteorological surface forcing, can we estimate the vertical mixing coefficient K_T in the upper ocean? As a first step, we study here the sensitivity of the surface phytoplankton concentration to the profile of the vertical mixing coefficient. Thereto we use an idealised phytoplankton growth model (Huisman and Sommeijer, 2002; Ryabov et al., 2010) together with the measured K_T profiles during the two cruises.

The paper is structured as follows. In Sect. 2, the relevant satellite data and the measurements of the STRATIPHYT cruises are presented. Next, in Sect. 3, the idealised phytoplankton growth model is presented and its calibration (e.g. parameter tuning) is discussed in Sect. 4. The main analysis of the sensitivity of the equilibrium phytoplankton distributions to the vertical mixing profiles appears in Sect. 5. Finally, in Sect. 6 the results are discussed and the conclusions are formulated.

2 Data

For the analysis presented in this paper, we use both satellite colour data as well as in situ data measured during the STRATIPHYT cruises. Additional information on this data can be obtained from http://oceancolor.gsfc.nasa.gov and http://projects.nioz.nl/stratiphyt, respectively.

2.1 Satellite data

During the past decades the range of applications for satellite data and their reliability has improved significantly. An important application is the measurement of Chl *a* surface concentration which can be used as a measure for the phytoplankton

OSD
11, 839–893, 2014

concentration close to the ocean surface. The data is based on the reflectance of blue and green wavelengths and can therefore only be obtained for the first meters of the water column. Figure 1b shows $1^\circ \times 1^\circ$ box averaged and monthly mean values of the Chl *a* surface concentration recorded by the MODIS on the Aqua satellite. To retrieve the Chl *a* concentrations from MODIS Aqua ocean colour data, the OC3 M algorithm (O'Reilly et al., 2000) is used. The data is plotted along the ship track in the North Atlantic during the STRATIPHYT cruises (shown in Fig. 1a) over the years 2009 to 2011. Black data points correspond to gaps in the data, e.g. due to high cloud coverage or the lack of sunlight. PAR was measured during the CTD casts of both STRATIPHYT cruises. Since these are very instantaneous measurements, which vary strongly not only with the daily cycle of the sun but also due to cloud coverage, daily mean Aqua MODIS Photosynthetically Available Radiation data was used for the PGM.

2.2 In situ data

During the two STRATIPHYT cruises in summer 2009 and spring 2011 the ship stopped multiple hours per latitudinal station which allowed the scientists to measure several depth profiles per station. Though these measurements give only snapshots into the vertical structure of the North Atlantic, there is evidence (Jurado et al., 2012b) that they are a good representation of the seasonal characteristics. We will therefore refer to the data sets of the 2009 and 2011 cruises as summer data and spring data, respectively.

The obtained temperature microstructure measurements were used to derive depth profiles for the vertical mixing coefficient (K_T [$m^2 s^{-1}$]) according to the Osborn (1972) model. K_T was computed from the temperature variance dissipation rate, χ_T [$°C s^{-1}$], according to

$$\chi_T = 6 D_T \overline{\left(\frac{\partial T'}{\partial z}\right)^2} \quad ; \quad K_T = \frac{\chi_T}{2} \left(\frac{\partial \overline{T}}{\partial z}\right)^{-2}, \tag{1}$$

OSD
11, 839–893, 2014

where D_T is the molecular diffusivity of heat ($\approx 1.4 \times 10^{-7}\,\mathrm{m^2\,s^{-1}}$) and $\partial\overline{T}/\partial z$ and $\partial T'/\partial z$ are the mean and fluctuation part of the temperature gradient (for details see Jurado et al., 2012b).

In Fig. 2 the station-mean, smoothed and interpolated profiles for K_T are shown for both cruises (Jurado et al., 2012a, b). Here, the profiles are smoothed over windows of 5 m depth to guarantee the compatibility with the numerical scheme used in the phytoplankton model, as will be explained below. The mixed layer depth (MLD, dashed line in Fig. 2) is defined as the depth at which the temperature difference with respect to the surface is 0.5 °C (Levitus et al., 2000). In spring, the MLD ranges between 20 m and 60 m for stratified stations up to 46° N. Further north, the water column is nearly homogeneously mixed. In summer, the profiles of the mixing coefficient show stratified characteristics for all stations with maximum values of the MLD around 45 m. The strength of the vertical mixing and its vertical properties change both seasonally as well as latitudinally.

In situ measurements of phosphorus and nitrogen show that there is a gradient in the nutricline between south and north (van de Poll et al., 2013). For simplicity we generalize the overall concentration of phosphorus, nitrogen, and nitrate as nutrients. According to the measured data, the water column provides sufficient nutrients for the phytoplankton to grow close to the surface in the northern stations, a so-called mesotrophic state. At stations further south the surface layer is practically depleted of nutrients and therefore oligotrophic. The transition between the oligotrophic and the mesotrophic stations lies at about 40° N during the spring cruise and at about 45° N during the summer cruise. The comparison with the Chl *a* profiles in Fig. 3 shows that these are also the latitudes of transition from an deep chlorophyll maximum (DCM) to an upper chlorophyll maximum (UCM).

For optical measurements, the fluorometer of a CTD profiler was used. Since PAR is absorbed by Chl *a* cells, fluorescence is used as a measure for the Chl *a* concentration (Suggett et al., 2011). In Fig. 3 the phytoplankton cell concentration measured during the spring and the summer cruise, respectively, are shown. The CTD profiles are based

OSD
11, 839–893, 2014

on the fluorescence in units of the Chelsea Aqua 3 Chl *a* concentration (g/l) and were measured down to depths of 200 m. The conversion from Chl *a* to cells is based on a combined conversion factor of Ryabov et al. (2010) and Omta et al. (2009) (see Sect. 4.1). Well-mixed stations, as in the north during spring, show a homogeneous distribution of phytoplankton cells over the first 100 m depth. Stratification forces the phytoplankton to grow either within the mixed layer and to form an UCM, or to grow below the mixed layer in a DCM.

Figure 3 as well as the MODIS Aqua data in Fig. 1b show that the transition from the UCM to the DCM happens later in the year and has a shorter duration the further north one observes the surface Chl *a* concentration. At latitudes north of 45° N surface concentrations remain relatively high throughout the entire light season, while regions south of 45° N exhibit very low Chl *a* concentrations during summer. Irrespective of the latitude, locally and temporally restricted surface Chl *a* maxima are also seen independent of the stratification cycle, e.g. in MODIS Aqua data, and these maxima have been suggested to be connected to ocean eddies (Mahadevan et al., 2012).

3 Phytoplankton growth model

The phytoplankton growth model (PGM) is based on the advection-reaction-diffusion models by Huisman and Sommeijer (2002) and Ryabov et al. (2010). Figure 4 provides a sketch of the basic model setup and the processes controlling growth and phytoplankton distribution in the model. Phytoplankton cells need nutrients and light to grow and their number is reduced at a constant rate representing sedimentation and grazing. Sunlight penetrates the water at the surface (yellow arrows) and its intensity decreases with depth due to the background attenuation of sea water and absorption by phytoplankton cells. Vertical mixing (blue arrows) is represented as a depth-dependent diffusion coefficient and it distributes nutrients (orange diamonds) and phytoplankton cells (green patches) over the water column.

OSD
11, 839–893, 2014

3.1 Governing equations

In a water column of depth Z_b the density of phytoplankton cells at time $t > 0$ and vertical position $z \in [0, Z_b]$, where $z = 0$ indicates the surface and z is positive downwards, is denoted by $P(z,t)$ (Fig. 4). The two controlling factors for phytoplankton growth are the concentration of nutrients $N(z,t)$ and the intensity of light $I(z,t)$. The coupling of nutrient and phytoplankton dynamics is described by the following two equations (Ryabov et al., 2010):

$$\begin{aligned}\frac{\partial P}{\partial t} &= \text{growth} - \text{loss} - \text{sinking} + \text{vertical mixing} \\ &= \mu(N,I)P - mP - v\frac{\partial P}{\partial z} + \frac{\partial}{\partial z}\left[K_T(z)\frac{\partial P}{\partial z}\right],\end{aligned} \tag{2}$$

$$\begin{aligned}\frac{\partial N}{\partial t} &= -\text{uptake} + \text{recycling} + \text{vertical mixing} \\ &= -\alpha\mu(N,I)P + \varepsilon\alpha mP + \frac{\partial}{\partial z}\left[K_T(z)\frac{\partial N}{\partial z}\right],\end{aligned} \tag{3}$$

where $\mu(N,I)$ describes the local growth. Furthermore, m is the mortality, v is the sinking velocity, $K_T(z)$ is the depth dependent vertical mixing coefficient, α is the nutrient content of a phytoplankton cell and ε is the nutrient recycling coefficient.

No flux conditions are assumed at the surface $z = 0$ for both the phytoplankton concentration and the nutrient concentration. At the bottom boundary, $z = Z_b$, the nutrient density is prescribed as constant value N_b, which represents a infinite source of nutrients in the deep ocean. The magnitude of this source is latitude dependent and based on measurements as discussed below and shown in Table 3. The initial phytoplankton concentration P is based on the measured profiles. Since Z_b lies well below the euphotic layer, the lower boundary condition for the phytoplankton concentration is kept at zero which is in agreement with the measurements. Further description as well as standard values of the parameters can be found in Table 1.

OSD
11, 839–893, 2014

Growth and loss couple P to N via the uptake of nutrients and the partial recycling of dead phytoplankton cells. The growth rate $\mu(N,I)$ has a strong local dependence on the available resources and is written as:

$$\mu(N,I) = \mu_{\max} \min\left(\frac{N}{H_N + N}, \frac{I}{H_I + I}\right), \quad (4)$$

where $\mu_{\max}$ is the maximum growth rate of phytoplankton and H_N and H_I are the half-saturation constants of nutrient limited and of light limited growth, respectively. For example, the value of H_N is relatively low for species which are well adapted to nutrient limited regimes.

The intensity of light as a function of vertical position z and time t is given by the Beer–Lambert's equation

$$I(z,t) = I_{in} \exp\left[-K_{bg} z - k \int_0^z P(\xi,t) d\xi\right], \quad (5)$$

where I_{in} denotes the intensity of the incoming light at the surface of the water column. The intensity of light within the water column decreases with depth due to a constant background attenuation represented by K_{bg} [m^{-1}]. Additionally, each phytoplankton cell absorbs photosynthetic active radiation which leads to a shading effect on the whole water column below the cell; this effect is represented by the term involving k [m^2 $cell^{-1}$]. Since $I(z_i,t)$ is dependent on phytoplankton concentrations at depths $z \leq z_i$, the PGM is a non-local model.

3.2 Numerical implementation

In the PGM, vertical mixing is defined by a prescribed vertical mixing profile $K_T(z)$ and here we make use of the measured vertical mixing profiles of K_T as presented in Sect. 2. As the bottom boundary of the model Z_b = 200 m, these profiles were extended to the depth of 200 m with the mean of the 10 deepest data points. Missing

OSD
11, 839–893, 2014

data points within the vertical profile were linearly interpolated from the nearest available data points. Finally the profiles were smoothed over windows of 5 m depth. This is done to guarantee the compatibility with the diffusion scheme used in the phytoplankton model.

In situ measurements of PAR at the water surface vary strongly and on time scales of hours and less. Therefore I_{in} is initialised with the daily mean Aqua MODIS PAR data on the date and at the location of the according station. Since we study steady state situations, I_{in} is kept constant during each model run. The initial nutrient concentration is assigned to the in situ profiles by van de Poll et al. (2013). While the vertical profile is changing according to Eq. (3), the bottom concentration N_b is kept constant to fulfill the boundary conditions. This value changes with latitude and season.

To solve the differential equations Eqs. (2) and (3) the NAG D02EJF routine (see for more details http://www.nag.co.uk) is used with a time step of 24 h. A grid spacing $\Delta z = 0.25$ m has to be applied to obtain sufficiently accurate solutions due to the strong vertical variation over some vertical mixing profiles. In all simulations, the model is run for a time interval of 500 days. The PGM adjusts to the environmental conditions within the first 50 to 100 days of the simulation. Thereafter variations in the system state happen mainly on time scales of the vertical mixing and the time to reach an equilibrium state can range from 100–1000 days. The in situ measurements did not only show strong seasonal variations but also moderate diurnal changes (not included here). Vertical mixing and therefore the environmental conditions on phytoplankton growth are therefore unlikely to maintain their major properties over periods longer than a few months. Our choice of 500 days is therefore a period which is long enough to equilibrate the system and which still represents a fairly realistic time frame of the relevant physical and biological processes.

Before generating the results with realistic vertical mixing profiles, we have compared the results of our version of the PGM with results in Huisman et al. (2006) and Ryabov et al. (2010). These computations have been done with homogeneous vertical mixing in the non-stratified case and an artificial vertical mixing profile in the stratified case

OSD
11, 839–893, 2014

(based on a generalized Fermi function, see Ryabov et al., 2010, for more details). The results in Huisman et al. (2006) show that the state of the phytoplankton profile is strongly dependent on the strength of the vertical mixing. The combination of light and nutrient limitation, sinking and low vertical mixing eventually leads to an unstable steady state and the amount of biomass undergoes a transition to an oscillatory state. Ryabov et al. (2010) studied the effect of stratification on the model state and forced the system into DCM and UCM states by changing the strength of the vertical mixing. We have performed similar studies with our version of the PGM and the results of the Ryabov et al. (2010) work could successfully be reproduced. The PGM is therefore capable to simulate different phytoplankton growth states dependent on the characteristics of the applied vertical mixing.

4 Calibration of the model

In the PGM various physical, optical, biological, and chemical parameters appear, as given in Table 1. The measurements allow us to calibrate most of these parameters. Optical parameters like K_{bg} and k can be determined by combining Eq. (5) to the measured light profile (see Appendix for a description of the method). In Sect. 4.1 the calibration of the values of these coefficients is presented. The values of the biological parameters affect the modelled growth behaviour of the phytoplankton. Many experiments and measurements are made to determine for example the growth rate of individual phytoplankton species in a specific environment (Peters et al., 2006). Results show that growth rates do not only vary between species but also due to environmental changes. The biological data of the STRATIPHYT project shows that the Chl *a* profiles originate from compositions of different phytoplankton species (van de Poll et al., 2013). Simulating the phytoplankton growth at STRATIPHYT stations by means of the PGM, in which growth is represented by a single species, requires calibration of the biological parameters to the measured data. In Sect. 4.2 the two main growth parameters, the half saturation constants of light limited growth and of nutrient limited growth, H_I

OSD
11, 839–893, 2014

and H_N, respectively, are calibrated to the in situ measurements. The results of the two calibration steps are discussed in Sect. 4.3.

4.1 Optical parameters k and K_{bg}

As described above, fluorescence is a measure of Chl *a* in water while in the PGM, phytoplankton is represented in cell numbers. The ratio of Chl *a* per cell can vary significantly depending on species and environmental conditions. Up to now there is no universal equation explaining this complex relation (Falkowski and Raven, 2007). Therefore a general ratio of 0.2×10^9 cells [µg Chl *a*]$^{-1}$ is chosen for simplicity. This ratio is based on the cell:nutrient content ratio and the nutrient content : Chl *a* ratio given by Ryabov et al. (2010) and Omta et al. (2009), respectively.

The transmittance of light in water can be affected by waves and a high concentration of small air bubbles at the surface as well as phytoplankton, sediments and dissolved organic material in the water column. It is beyond the scope of this work to quantify all these effects. Since surface effects are very localised and sediment concentrations are very low in open water they are both not taken into account in the analysis. Our aim is rather to identify the characteristics of the light attenuation due to the two major contributions as represented by K_{bg} and k in Eq. (5).

In Eq. (5) the dependence of the light intensity is given as an exponential function of depth. Figure A1 in the Appendix shows an example of a vertical CTD profile measuring fluorescence (green), surface irradiance (red), and corrected irradiance (blue, logarithmic scaling). A very defined DCM is located at around 65 m depth. To deduce the values of K_{bg} and k from such measurement data the light profile is divided into two sections: a Chl *a* free section at the bottom of the euphotic layer and a section of a high Chl *a* concentration in the euphotic layer. The first section is used to determine the attenuation only based on K_{bg}. It is indicated by the blue interval in Fig. A1 and in the following referred to as "blue section". The second section serves to estimate the phytoplankton related attenuation based on a depth section ranging from half of the maximum concentration above to half of the maximum concentration below

OSD
11, 839–893, 2014

the maximum concentration of phytoplankton. This section is referred to as the "green section" since it corresponds to the green shaded area in Fig. A1.

Making use of these localised properties of phytoplankton the quantities K_{bg} and k are determined in two steps. First K_{bg} is calculated based on the blue section in which the phytoplankton concentration has no influence (since it is approximately zero). In the second step, k is determined over the green section with high phytoplankton concentration using the K_{bg} value obtained at the first step. Details of the calculations are presented in the Appendix.

In the Fig. A3 the results of K_{bg} for the STRATIPHYT spring and summer cruises can be seen. For most stations multiple measurement profiles were available and the data points shown are the mean values per station. The error bars in the graphs are based on the standard deviation between different profiles for one station. Stations defined by DCM states (south of the red dashed line in Fig. A3) show values for K_{bg} in the range of $0.032\,m^{-1}$. In stations with an UCM (north of the red dashed line and south of the green dashed line) the backscattering effect of particles could lead to an increased absorption effect which affects the K_{bg} value since the backscattering is not implicitly taken into account in our method (further details can be found in Siegel et al. (2005)). At northern latitudes of the spring cruise (north of the green dashed line) the Chl *a* is homogeneously mixed over the entire measured depth. Therefore no blue section can be defined and hence K_{bg} cannot be determined.

Applying the resulting mean K_{bg} found for the DCM states, k is determined based on the green section of the Chl *a* profiles; results are shown in Fig. A2. For the summer data, values of k show a mean of $5.9 \pm 1.9 \times 10^{-10}\,m^2\,cell^{-1}$. The mean k derived from the spring data is more than twice as high and to take both seasons into account a value of $k = 10^{-9}\,m^2\,cell^{-1}$ is chosen.

OSD
11, 839–893, 2014

4.2 Growth parameters H_I and H_N

To calibrate the parameters H_I and H_N such that the PGM reproduces the main features of the measured Chl *a* profile, we assume that all measured profiles are in a steady state. The Least Squares Method (LSM) as implemented in the NAG E04FCF (an unconstrained optimization solver) is used. We choose two stations of the summer cruise with different steady states: a DCM and a UCM. The DCM corresponds to measurements at the southern part of the track at 40.5° N and the UCM to a more northern station at 60.7° N. These stations are in the following referred to as the southern and northern station, respectively. Additionally, a third station of the spring cruise at 45.5° N is chosen which shows a significant UCM in spring and a DCM in summer with still a relative high surface concentration of Chl *a* (see Fig. 3). Because of this state change with the seasons we refer to it as the transition station.

The reference phytoplankton profiles are found in two different states: DCM and UCM. To define the residuals in the LSM, basic characteristics of the different phytoplankton profiles have to be defined. In case of a DCM we choose the depth of the DCM and its associated maximum phytoplankton concentration as the two major characteristics. In a UCM state, the phytoplankton cells are spread out over a wider depth range and hence the mean phytoplankton cell concentration and the mean nutrient concentration within the mixed layer are used. For each characteristic C^i, the normalized difference between measured C^i_{obs} and model determined C^i_{mod} value is used as a residual in the LSM and the sum of squares S is given by

$$S = \sqrt{\sum_i \left(1 - \frac{C^i_{\mathrm{mod}}}{C^i_{\mathrm{obs}}}\right)^2}. \quad (6)$$

OSD
11, 839–893, 2014

4.2.1 The southern station

In Fig. 5 the biological, chemical, optical, and physical data profiles are shown for the southern station at (13.2° W, 40.5° N) on 23 July 2009. The green profile in the left panel gives the phytoplankton concentration with a maximum at around 60 m depth, clearly showing a DCM. The nutrient concentration (red dashed line) combines the measured concentrations of phosphate (PO_4), nitrogen dioxide (NO_2), and nitrate (NO_3) in one. The main source of these nutrients is deeper, nutrient rich water (van de Poll et al., 2013) and it is clearly visible that the mixed layer is depleted of nutrients. Note that the light intensity profile (blue dashed line) is plotted with logarithmic scaling. Data is only available after a depth of 5 m. The light intensity decays exponentially and has very low values at depths of the DCM and further below. The vertical turbulent mixing profile shows high values close to the surface decaying rapidly at a depth of approximately 25 m.

In Fig. 6a the interpolated result for the sum of squares S, based on the depth and maximum value of P at the DCM, is plotted vs. H_I and H_N. High values of S are plotted in red and resemble PGM results (based on a certain set of H_I and H_N) that are very different from the in situ profiles. Blue areas define sets of half-saturation constants for which the PGM result lies close to the observations. Note that the interpolation applied leads to a smoothing of the values of S and is only chosen to show the complexity of the calibration of H_I and H_N.

As can be seen in the center panel of Fig. 6b, the best match was achieved for the half-saturation constants $H_I = 57\,\mu\text{mol photons}\,\text{m}^{-2}\,\text{s}^{-1}$ and $H_N = 0.54\,\text{mmol nutrients}\,\text{m}^{-3}$. This figure does not only show that the system needs some time to adjust to the boundary conditions, but also demonstrates the effect of the half saturation constants on the properties of the phytoplankton profile. Increasing (H_I, H_N) from (57, 0.54) (blue line) to (80, 1.5) (green line) for example does not have a big effect on the depth of the DCM (top) but leads to a substantial decrease of the maximum concentration of phytoplankton cells at the DCM.

OSD
11, 839–893, 2014

4.2.2 The northern station

In Fig. 7a the biological, chemical, optical, and physical data profiles are shown for the northern station at (19.3° W, 60.7° N) on 8 August 2009. The green line in the first panel on the left shows the phytoplankton concentration with a high cell concentration at the surface spreading over the whole mixed layer. The nutrient concentration (red dashed line) combines again concentrations of phosphate (PO_4), nitrogen dioxide (NO_2) and nitrate (NO_3) in one. In contrast to the southern station, the mixed layer is not completely depleted of nutrients though their concentrations are very low. Below the mixed layer the nutrient concentration increases quickly to its bottom value. The light intensity profile (blue dashed line) is again presented using a logarithmic scaling. The values measured are almost half of what is measured at the southern station and the intensity decreases quickly over depth due to the high phytoplankton cell concentration within the mixed layer. The turbulent vertical mixing profile (right panel) differs from the one at the southern station since the strongest peak of mixing is located below the mixed layer.

The temporal evolution of the residuals of the LSM is shown in Fig. 7b as the plot of the nutrient residual (top), the sum of squares (center), and the phytoplankton residual (bottom). All plots show that the model adjusts quickly and the absolute minimum was detected for $H_I = 80\,\mu\text{mol photons}\,\text{m}^{-2}\,\text{s}^{-1}$ and $H_N = 2.5\,\text{mmol nutrients}\,\text{m}^{-3}$. The residual based on the mean phytoplankton concentration in the mixed layer indicates that the sensitivity to the change of the parameters is rather low in comparison to the sensitivity of the mean nutrient concentration (mind the different scales). Note that the minimum value of S achieved in this system has a value of about 0.09 while in case of the southern station S is of the order of 10^{-5}.

4.2.3 The transition station

In Fig. 8a the biological, chemical, optical, and physical data profiles are shown for the transition station at (12.9° W, 45.5° N) on 21 April 2011. In the left panel the

OSD
11, 839–893, 2014

phytoplankton concentration (green line) shows an UCM with lower concentrations than for the northern station. The light intensity (blue dashed, logarithmic scale) decreases strongly with depth due to the high phytoplankton concentration. The nutrient concentration (red dashed line) in the mixed layer is very inhomogeneous which could be a measurement artifact because the strong vertical mixing at these depths is expected to lead to a more homogenous distribution. Nonetheless nutrients are abundant in the mixed layer in contrast to the two reference stations in summer. The vertical mixing profile (right panel) also differs from the other reference stations and shows a deeper mixed layer and essentially stronger mixing. This suggests that during spring the vertical mixing provides more nutrients to the euphotic layer.

The transition station is characterised by an UCM and therefore the mean P and the mean N in the mixed layer are used to define the sum of squares S in the LSM. In the center panel of Fig. 8b, the best result is found for the parameter set $H_I = 2\,\mu\text{mol photons}\,\text{m}^{-2}\,\text{s}^{-1}$ and $H_N = 7.5\,\text{mmol nutrients}\,\text{m}^{-3}$. The temporal evolution of S (Fig. 8b center) shows that the system properties are still subject to relatively strong changes and the steady state is uncertain. In contrast, the parameter set $H_I = 70\,\mu\text{mol photons}\,\text{m}^{-2}\,\text{s}^{-1}$ and $H_N = 2.0\,\text{mmol nutrients}\,\text{m}^{-3}$ achieves better results for the mean nutrient concentration in the mixed layer (see dashed dark grey line in Fig. 8b top) but shows an overall weaker performance due to the too high mean phytoplankton concentration (dashed dark grey line in Fig. 8b bottom). Since we are in the end more interested in a good representation of the UCM and therefore a low residual in the mean phytoplankton concentration the most solid and representable choice appears to be the parameter set $H_I = 125\,\mu\text{mol photons}\,\text{m}^{-2}\,\text{s}^{-1}$ and $H_N = 3.0\,\text{mmol nutrients}\,\text{m}^{-3}$ (turquoise lines). Keeping in mind the previous LSM results, as well as the fact that the system with the lowest sum of squares S is far from being steady (blue line), this parameter set is chosen to represent growth properties at the transition station.

OSD
11, 839–893, 2014

4.3 Discussion on the model calibration

As comparing the results of highly idealised models, such as the PGM, to in situ measurements and use them for calibrating models parameters may raise concerns (see e.g. Evans et al., 2013), we provide in this section a rather extensive discussion of the model calibration results. This discussion is important for the sensitivity analysis in the next section, which is dedicated to the sensitivity of the PGM to different vertical mixing profiles.

In general all values for K_{bg} as well as for k, shown in the Figs. A2 and A3, lie in the range of values used in other models (see Table 2). The relatively high values for the standard deviation at some stations can be partially explained by the varying fraction of light which is reflected at the surface due to the zenith angle. When the sun stands low, a higher fraction of the incoming light will be reflected already at the water surface (Mobley, 1994; Kirk, 2011). This effect leads to a lower ratio of the intensity of light in the water column to the intensity of the incoming light and is primarily independent of the optical properties of the water column. To avoid extreme influence of the solar angle, data measured early in the morning and late in the afternoon are not taken into account. The values of K_{bg} during the summer cruise (Fig. A3a) are characterised by two different domains. In southern stations with a well-defined DCM (latitudes up to 49° N, south of the dashed line in Fig. A3a) values of K_{bg} are close to their mean of $0.032\,m^{-1}$. For more northern stations with phytoplankton distributions dominated by a UCM, K_{bg} increases with increasing latitude. A possible explanation of this difference is the effect of particulate backscatter which becomes more important at higher latitudes (Siegel et al., 2005).

The analysis of the optical properties during the spring cruise is mainly limited to the DCM stations (south of the red line in Fig. A3). For homogeneously mixed stations our method cannot be used since it is impossible to distinguish between the effect of phytoplankton absorption and K_{bg} in such systems. The results in Fig. A3 show that K_{bg} values are more spread for the spring cruise and the standard deviation can be

OSD
11, 839–893, 2014

up to 100 %. Still most of the values are close to the value of the $0.032\,m^{-1}$ which is determined based on the summer data. This value of K_{bg} is also consistent with those determined from the detailed (spectrally resolved) measurements in the clearest oceanographic waters (Morel et al., 2007) and hence we adopted this value for the PGM.

Figure A2 shows that the derived k based on the spring data shows higher values as well as a wider spread compared to the results based on the summer data. The origin of these high variations can be manifold (e.g. the biological composition and species dependent properties) and an explanation is outside the scope of this paper. The strong consistency of the summer results and the comparison with the literature (see Table 2) would suggest to choose $k = 6.0 \times 10^{-10}\,m^2\,cell^{-1}$ for the PGM. Instead a more general value of $10^{-9}\,m^2\,cell^{-1}$ is chosen which is the mean of the spring and the summer result. The motivation for this k value lies again in the model assumption that the total phytoplankton growth is idealised as one species.

Applied to the southern station, the LSM leads to $H_I = 58\,\mu mol\,photons\,m^{-2}\,s^{-1}$ and $H_N = 0.5\,mmol\,nutrients\,m^{-3}$. Both values lie in the range of commonly used parameters as can be seen in Table 2. The half saturation constants for both UCM stations have higher values. The northern station is characterised by $H_I = 80\,\mu mol\,photons\,m^{-2}\,s^{-1}$ and $H_N = 2.5\,mmol\,nutrients\,m^{-3}$ and the transition station by $H_I = 125\,\mu mol\,photons\,m^{-2}\,s$ and $H_N = 3\,mmol\,nutrients\,m^{-3}$. In case of the light limitation, these values are up to one order of magnitude higher than those found in literature. The values of H_N are of the same order of magnitude as the one of Fiechter (2012) but are two orders of magnitude larger than those used in other parameterisations (cf. Table 2).

In the case of the UCM the mean values of P and N in the mixed layer have to match the in situ data. From Eq. (3), we can see that the uptake and recycling should therefore be in balance (assuming that the vertical mixing is not a dominant factor as soon as the steady state is reached). With the additional use of Eq. (4) this leads to the following

OSD
11, 839–893, 2014

steady state condition:

$$\left\langle \overline{\min\left(\frac{N}{H_N+N}, \frac{I}{H_I+I}\right)} \right\rangle_{ML} \approx \frac{\varepsilon m}{\mu_{max}}, \quad (7)$$

where $\overline{\langle a \rangle}_{ML}$ is the vertical average of a over the mixed layer. The right hand side of Eq. (7) leads to 0.125 for the parameters given in Table 1 which sets also the mean growth limiting factor over the mixed layer, as given by the left hand side of Eq. (7). Figure 9a shows the vertical profiles of the system properties as derived by the LSM for the northern station. The light intensity is plotted in blue, the nutrient concentration in red, and the phytoplankton concentration in green. The dashed blue and red lines indicate the values of H_I and H_N, respectively while the dashed grey line defines where the system changes from a nutrient limited growth (above) to a light limited growth (below). Figure 9b shows that the resulting growth limiting factor is strongly coupled to the shape of the limiting resource.

Equation (7) can be used for a crude estimate for the half saturation constants in this case. The mean nutrient concentration over the mixed layer is 0.61 mmol nutrients m^{-3}. Assuming that the nutrients would be the only growth limiting factor in the mixed layer leads to $H_N \approx 4.3$ mmol nutrients m^{-3}. The light intensity close to the surface is relative high but decreases fast due to the high phytoplankton concentration. In the case of an incoming light intensity of 390 µmol photons m^{-2} s^{-1} this would roughly lead to a half saturation constant of light limited growth $H_I = 100$ µmol photons m^{-2} s^{-1} (in absence of nutrient limitation). Both of these estimates have relatively high values which provides support that the simplified growth function in combination with the available resources leads to the high values of H_N and H_I (as obtained with the LSM).

In a system with a very high nutrient limitation, the main growth is pushed deeper to a depth where nutrient concentrations are higher and light becomes the limiting factor. Analysis of the growth function of DCM profiles showed that the upper part of the phytoplankton growth is always nutrient limited. In Fig. 10a the vertical profiles of the

OSD
11, 839–893, 2014

system properties of the southern station are shown. The dashed grey line indicates the transition from one limiting resource to another at about 60 m depth. Growth above this depth is limited by the low nutrient concentration (red line). Since light intensity decreases strongly with depth it becomes the limiting factor below the grey line. The depth of the maximum is therefore defined by H_N while the light limits the growth further below. In a steady state with a DCM, the mean value on the left hand side of Eq. (7) would have to be replaced by the nutrient concentration and light intensity at the depth of the DCM (see also Fennel and Boss, 2003). In the case of nutrient limited growth, this leads to $H_N = 2.6\,\mathrm{mmol\,nutrients\,m^{-3}}$ which is larger than that determined by the LSM. The low vertical mixing below the mixed layer enhances the effect of sinking on the steady state of the phytoplankton distribution (Huisman et al., 2006). This is not taken into account in Eq. (7) and its effect would lead to a decrease in H_N.

Figure 10b shows the resulting growth factor which is computed by the minimum given in Eq. (4) and has to be multiplied by μ_{max} to give the final growth rate. The shape of the growth factor is defined by the local availability of the limiting resource. Therefore it remains constant over the mixed layer, where nutrients are limiting, increases with depth like the nutrient concentration and decreases exponentially below 60 m where the low light intensity limits growth.

In order to test the robustness of the determined parameters a series of sensitivity tests have also been done. The tests are all based on the standard model setup with the calibrated parameter values. Biological parameters, like the growth rate and the recycling rate, as well as N_b and I_{in} have been varied (one at the time) over a range of realistic values as measured or used in the literature. The most important outcome of this study is that none of these parameter variations shows any unexpected growth dynamics. The phytoplankton concentrations at the southern station respond generally quicker to changes in the biological or environmental parameters than those at the northern and the transition stations. The tests also a show high sensitivity to parameters which connect to the nutrient content of the system, like the nutrient concentration at the bottom of the system and the recycling coefficient. While the first is determined

OSD
11, 839–893, 2014

by measurements, the latter involves more complex processes like grazing, remineralisation and sedimentation. Further model studies about the recycling coefficient would therefore be interesting but are not carried out as part of this work.

5 Sensitivity to turbulent vertical mixing

After having discussed the calibration of the parameters in the PGM at the three reference stations we now turn to the study of the sensitivity of the modelled phytoplankton distribution to turbulent vertical mixing. In Sect. 2.2 the observed vertical mixing coefficients along the zonal transect from 29° N to 63° N for the STRATIPHYT cruises in summer 2009 and spring 2011 were presented. These are all realisable mixing profiles determined by the particular surface forcing and background stratification. In this section all available vertical mixing profiles (for both spring and summer cruises) are used in the PGM at each of the three reference stations. The other parameters and boundary conditions are fixed as calibrated at the single reference stations. For each case, the PGM is integrated for 500 days; in this way any change of the equilibrium phytoplankton response can be directly connected to the changes in the vertical mixing profile.

5.1 Phytoplankton profiles

The phytoplankton concentrations shown in Fig. 11 are PGM results for the southern station (see Table 3). The latitude in this figure refers to the applied vertical mixing profile (as shown in Fig. 2) which is used at the southern station. The red box marks the reference station to which the model parameters are calibrated. Vertical mixing profiles of the spring cruise, which are mainly characterised by strong mixing, lead to a DCM (using the profile from the southmost stations) and a series of UCMs which become shallower up to 46° N and appear to correlate with the MLD. North of 50° N, the strong vertical mixing leads to states with a homogeneously populated euphotic layer of which some have very low phytoplankton concentrations. The results for the

OSD
11, 839–893, 2014

summer mixing profiles show solely DCMs whose depth, spread, and intensity vary strongly. There is no clear correlation of the DCMs with the MLD in this case.

In Fig. 12 the modelled phytoplankton concentrations are shown for the northern station. The upper panel shows the PGM results for the vertical mixing profiles measured during the spring cruise. Vertical mixing profiles from all stations in the southern part of the transect show an UCM and those from stations north of 50° N (with strong mixing) give a homogeneously distributed phytoplankton concentration. These results are very similar to the results obtained based on the southern reference station (cf. upper panel of Fig. 11).

However, the application of vertical mixing profiles from the summer cruise to the northern station (lower graph in Fig. 12) shows completely different phytoplankton states than those for the southern reference station (cf. lower panel of Fig. 11). Most of the vertical mixing profiles lead to a UCM except for 3 from vertical mixing at the northern part of the transect (at 54° N, 58° N and 60° N). In comparison to the DCMs found for the southern station (Fig. 11), the DCMs found for the northern station are located directly below the mixed layer and the two southern ones of those are associated with relatively high surface Chl *a* concentrations.

In case of the transition station, the resulting phytoplankton profiles computed with the PGM for the different vertical mixing profiles can be seen in Fig. 13. The upper (lower) panel shows again the results for the spring (summer) vertical mixing profiles. For latitudes up to 46° N, the vertical mixing profiles during spring lead all to UCM states with varying intensity and a depth correlated with the MLD. Northern vertical mixing profiles of the spring cruise give homogeneously distributed phytoplankton profiles. Phytoplankton concentrations calculated using the summer mixing profiles result in both DCM and UCM states with no clear latitudinal dependence. Both UCM and DCM states seem to be related to the depth of the mixed layer with the highest phytoplankton concentration in the mixed layer or just below it.

OSD
11, 839–893, 2014

5.2 Bulk and surface sensitivity

The results from the previous subsection indicate that the phytoplankton concentration at each of the reference stations is sensitive to the vertical mixing profile. The challenging task is now to identify the major controlling processes and characteristics of the vertical mixing which lead to this range in phytoplankton concentrations.

The phytoplankton distributions at the three reference stations having either a UCM or a homogeneous profile are best compared by the upper 20 m mean surface phytoplankton concentration, here indicated by P_s. Values of P_s (Fig. 14a) computed from the results in the Figs. 11–13 lie in the range of 0.5–1.6 $\times 10^8$ cells m^{-3} for the vertical mixing profiles south of 50° N and between 1–7 $\times 10^7$ cells m^{-3} for the homogeneously mixed profiles (north of 50° N). The strong vertical mixing at 60° N leads to extinction of phytoplankton for the transition station and the northern station. Values of P_s by these two reference stations show overall a similar behaviour vs. vertical mixing (labeled with their initial latitude.

For the southern station, values of P_s are more sensitive to the different vertical mixing profiles. Phytoplankton profiles determined with strong vertical mixing (e.g. the homogeneously mixed profiles) lead to larger P_s values at the southern station than those at the other two reference stations. Growth in these cases is generally limited by light and the high I_{in} and the low H_l values induce larger growth rates at the southern station. In addition, N_b is relatively low at the southern station which makes the phytoplankton growth more sensitive to a reduction of the vertical mixing (e.g. profiles between 40° N and 50° N).

For the summer mixing profiles, DCM states appear at the southern station while the northern station is dominantly found in an UCM. In this case the depth of the DCM found for each reference station is plotted in Fig. 14b. As UCM states are not shown in this graph, the northern station is only represented by two vertical mixing profiles. Even though the value of H_N of the southern station is only a fraction of the H_N of the transition station, the low N_b value is limiting growth to larger depths (mainly below

OSD
11, 839–893, 2014

50 m) for the southern station. The transition and the northern station are less nutrient limited for the same vertical mixing since the N_b value is higher in both cases. Therefore their PGM results show shallower DCM states (or even UCM states) than the southern station.

To distinguish light limited and nutrient limited regimes the position of the nutricline, which is defined as the depth of the highest gradient in the vertical nutrient concentration, can be used. For the results in the Figs. 11–13, the total biomass is plotted vs. the depth of the nutricline in Fig. 15a. When the nutricline is closer to the surface more light is available to the phytoplankton cells and this leads to an increase of the total biomass. PGM states which are not limited by nutrients are plotted along the y axis since these do not have a nutricline.

All these results suggest that the vertical mixing as well as the boundary condition N_b play a very important role in the supply of nutrients to the euphotic layer. To obtain a quantitative measure of the change in vertical nutrient flux due to changes in the vertical mixing profile, a (dimensionless) relative nutrient flux ρ_N^i is defined as:

$$\rho_N^i = \frac{\overline{-K_T^i(z)\frac{\partial N^i}{\partial z}}}{\overline{\left[-K_T(z)\frac{\partial N}{\partial z}\right]_{\text{ref}}}} \approx \frac{\sum_{j=0}^{J-1}\left[K_T^i(z_j)\left(N^i(z_{j+1}) - N^i(z_j)\right)\right]}{\sum_{j=0}^{J-1}\left[K_T(z_j)(N(z_{j+1}) - N(z_j))\right]_{\text{ref}}}. \quad (8)$$

where J is the number of grid points in the vertical and the bar indicates vertical averaging. For every vertical mixing profile $K_T^i(z)$ the relative nutrient flux ρ_N^i gives a measure of the nutrient flux based on the station specific vertical mixing, where i defines one of the M vertical mixing profiles and $N^i(z)$ is the corresponding nutrient density at depth z. The denominator normalises the flux with the nutrient flux of a particular reference station (e.g. the southern station) from which it follows that ρ_N^{ref} is equal to one.

For the three reference stations, the values of P_s are plotted vs. ρ_N^i in Fig. 15b for only the nutrient limited cases (cf. in Fig. 15a). The values of P_s are normalised by the maximum value of each reference station. In all three cases P_s increases with increasing nutrient flux showing the sensitivity of the surface phytoplankton concentration to

OSD
11, 839–893, 2014

the vertical mixing profiles through the relative nutrient flux. In case of the southern station, the reference nutrient flux is very low due to the weak summer mixing at 41° N. This leads to high values of ρ_N^i for spring vertical mixing and hence a different scale is used for ρ_N^i in Fig. 15b.

6 Summary and discussion

In this work, we used in situ measurements of the STRATIPHYT project to calibrate the PGM and subsequently used this model to study the sensitivity of the phytoplankton distribution to vertical mixing profiles. A discussion of the calibration of the parameters in the PGM was already given in Sect. 4.3. We are confident that the three parameter sets for the different reference stations are a good choice to represent characteristic phytoplankton growth in the PGM.

When compared to in situ as well as to the ocean colour data, the phytoplankton concentrations for the deep DCM states are up to 2 orders of magnitude too low. However, the model results for shallow DCM states and for UCM states are of the same order as the measurements. To retrieve the Chl *a* concentrations from MODIS Aqua ocean colour data, the OC3M algorithm was used. Comparisons to in situ measurements have shown that this algorithm underestimates Chl *a* concentrations below 1 mg m^{-3}, and overestimates them at larger values. In the latter case this would mean that our model might perform even better at high concentrations than the comparison would suggest. On the other hand the performance at low concentration may be poorer (see Martin, 2004, and http://oceancolor.gsfc.nasa.gov/ for more details).

To study the sensitivity of these three different reference model situations to the vertical mixing profile, we keep all parameters as calibrated for each station fixed and apply the vertical mixing profiles shown in Fig. 2. Resulting changes in the modelled phytoplankton growth at each of the three reference stations are therefore only due to the changes in the vertical mixing. For summer mixing profiles, the southern station shows only DCM states while the northern station remains mainly in the UCM state.

OSD
11, 839–893, 2014

The transition station is found in both of these states depending on the vertical mixing profile. Results for the spring mixing profiles are less divers because the vertical mixing profiles in stratified cases are characterised by stronger mixing than in the summer data. The stronger supply of nutrients from depth leads to the formation of a UCM for almost all PGM results.

The model results show the importance of vertical mixing for the nutrient supply to the euphotic layer. Nutrient limited stations of all three reference stations show an increase in total biomass with the shallowing of the nutricline. To connect this effect to properties of the vertical mixing the relative nutrient flux is defined. With this measure we are able to directly correlate the increase of surface phytoplankton concentration to the strength of the vertical mixing and its impact on the nutrient supply.

In summary, the results presented here demonstrate a strong sensitivity of phytoplankton distributions to observed vertical mixing profiles. In particular, there is a strong variation in the surface phytoplankton values with vertical mixing. The latter result suggests that data-assimilation techniques may be useful to constrain properties of turbulent vertical mixing with the help of surface Chl *a* concentrations. However, the results also indicate that this will be challenging as the surface concentration in the case of the modelled DCM is in most cases underestimated and has also a strong variation. This weak result in combination with the fact that DCM states are hard to determine from satellite data, is quite a challenge to overcome but certainly worth a try.

Appendix A

Calculation of k and K_{bg}

Figure A1 shows a DCM based on a vertical CTD profile measuring fluorescence (green, corrected irradiance (blue) and the surface irradiance (red). The corrected irradiance is the percentage of the instantaneous surface light intensity measured at depth. Since the surface irradiance can vary strongly on short timescales (here it increases

OSD
11, 839–893, 2014

during the measurement time, probably due to change in cloud coverage), the depth profiles of the light measurements are corrected to the instantaneous surface irradiance. Therefore the corrected irradiance is independent of the shading effects of clouds or other obstacles and a more representative measure for the transmittance of the water. The x axis goes from 0 (surface) to 250 m depth. At depths below 140 m the fluorescence signal shows slightly varying values above zero. These appear due to measurement artefacts, the so-called dark current, and Chl *a* concentrations can be assumed to be very low or even zero here.

The phytoplankton free depth section is indicated by z_1 and z_2 at approximately 142 m and 170 m depth, respectively. Writing Eq. (5) for any 2 points z_1 and z_2 within this interval will lead to an integral over $P(z)$ in the exponent of the Eq. (5), which has for all of these depths the same value since there is no additional phytoplankton found below 142 m. Therefore the integral can be replaced by the constant term P_{tot} which is used in a next step to eliminate the k-dependency by substituting the natural logarithm of the light intensity (Eq. 5) at depth z_2 into the one at depth z_1. Rearranging this equation then results in

$$K_{\mathrm{bg}} = \frac{\log\left(\frac{I(z_1)}{I_{\mathrm{in}}(z_1)}\right) - \log\left(\frac{I(z_2)}{I_{\mathrm{in}}(z_2)}\right)}{z_2 - z_1} \tag{A1}$$

which gives an estimate of K_{bg} for the given station.

As soon as a value for K_{bg} is found, the effect of the phytoplankton density distribution within the water column can be addressed. To do so, another section $[z_3, z_4]$, which contains a high concentration of phytoplankton cells, is defined. Here we choose the depths in which the phytoplankton density reaches half of its maximum value, above and below the depth of the maximum phytoplankton density. In Fig. A1 this section is defined by depths around 58 m and 72 m depth, respectively. We first write Eq. (5) for both depths z_3 and z_4 and take the logarithm of both equations (which linearises the dependency on k). Substituting the two resulting equations leads to the following

OSD
11, 839–893, 2014

equation:

$$\log\left(\frac{I(z_3)}{I_{\text{in}}(z_3)}\right) - \log\left(\frac{I(z_4)}{I_{\text{in}}(z_4)}\right)$$
$$= -K_{\text{bg}}(z_3 - z_4) - \left(\int_0^{z_3} kP(\zeta)\,\mathrm{d}\zeta - \int_0^{z_4} kP(\zeta)\,\mathrm{d}\zeta\right). \quad \text{(A2)}$$

The term in brackets on the right hand side of Eq. (A2) can be combined into one integral. To calculate the integral numerically, we use the trapezoidal rule given by

$$P_{\text{PEAK}} = \int_{z_3}^{z_4} P(\zeta)\,\mathrm{d}\zeta \approx 0.5\left(P(z_3) + 2\sum_{n=z_3+1}^{z_4-1} P(n) + P(z_4)\right) \quad \text{(A3)}$$

which gives the total amount of phytoplankton P_{PEAK} within the section $[z_3, z_4]$. Rearranging Eq. (A2) gives an expression for the absorption coefficient of phytoplankton k as:

$$k = \frac{1}{P_{\text{PEAK}}}\left(K_{\text{bg}}(z_3 - z_4) + \log\left(\frac{I(z_3)}{I_{\text{in}}(z_3)}\right) - \log\left(\frac{I(z_4)}{I_{\text{in}}(z_4)}\right)\right). \quad \text{(A4)}$$

Acknowledgements. Special thanks go to Elena Jurado for her help with the STRATIPHYT data, to Corina Brussaard, the chief scientist of the two STRATIPHYT cruises, and the crew of the R/V *Pelagia*. This work was funded by the NSO User Support Programme under Grant ALW-GO-AO/11-08 through the COLOURMIX project with financial support of the Netherlands Organization for Scientific Research (NWO).

OSD
11, 839–893, 2014

References

Antoine, D., Morel, A., Gordon, H., Banzon, V., and Evans, R.: Bridging ocean color observations of the 1980s and 2000s in search of long-term trends, J. Geophys. Res., 110, C06009, doi:10.1029/2004JC002620, 2005. 841

Behrenfeld, M. J.: Abandoning Sverdrup's Critical Depth Hypothesis on phytoplankton blooms, Ecology, 91, 977–989, doi:10.1890/09-1207.1, 2010. 841

Behrenfeld, M. J., O'Malley, R. T., Siegel, D. A., McClain, C. R., Sarmiento, J. L., Feldman, G. C., Milligan, A. J., Falkowski, P. G., Letelier, R. M., and Boss, E. S.: Climate-driven trends in contemporary ocean productivity, Nature, 444, 752–755, doi:10.1038/nature05317, 2006. 841

Boyce, D. G., Lewis, M. R., and Worm, B.: Global phytoplankton decline over the past century, Nature, 466, 591–596, doi:10.1038/nature09268, 2010. 840, 841

Doney, S. C.: Oceanography: plankton in a warmer world, Nature, 444, 695–696, doi:10.1038/444695a, 2006. 841

Evans, M. R., Grimm, V., Johst, K., Knuuttila, T., de Langhe, R., Lessells, C. M., Merz, M., O'Malley, M. A., Orzack, S. H., Weisberg, M., Wilkinson, D. J., Wolkenhauer, O., and Benton, T. G.: Do simple models lead to generality in ecology?, Trends Ecol. Evol., 28, 578–583, doi:10.1016/j.tree.2013.05.022, 2013. 857

Falkowski, P. and Raven, J.: Aquatic Photosynthesis, 2nd Edn., Princeton University Press, Princeton, 2007. 851

Fennel, K. and Boss, E.: Subsurface maxima of phytoplankton and chlorophyll: steady-state solutions from a simple model, Limnol. Oceanogr., 48, 1521–1534, 2003. 860

Fiechter, J.: Assessing marine ecosystem model properties from ensemble calculations, Ecol. Model., 242, 164–179, doi:10.1016/j.ecolmodel.2012.05.016, 2012. 858, 874

Huisman, J. and Sommeijer, B.: Population dynamics of sinking phytoplankton in light-limited environments: simulation techniques and critical parameters, J. Sea Res., 48, 83–96, doi:10.1016/S1385-1101(02)00137-5, 2002. 843, 846, 874

Huisman, J., Thi, N., Karl, D., and Sommeijer, B.: Reduced mixing generates oscillations and chaos in the oceanic deep chlorophyll maximum, Nature, 439, 322–325, doi:10.1038/nature04245, 2006. 849, 850, 860

OSD
11, 839–893, 2014

Johnk, K. D., Huisman, J., Sharples, J., Sommeijer, B., Visser, P. M., and Stroom, J. M.: Summer heatwaves promote blooms of harmful cyanobacteria, Glob. Change Biol., 14, 495–512, doi:10.1111/j.1365-2486.2007.01510.x, 2008. 842

Jurado, E., Dijkstra, H. A., and van der Woerd, H. J.: Microstructure observations during the spring 2011 STRATIPHYT-II cruise in the northeast Atlantic, Ocean Sci., 8, 945–957, doi:10.5194/os-8-945-2012, 2012a. 842, 845

Jurado, E., van der Woerd, H. J., and Dijkstra, H. A.: Microstructure measurements along a quasi-meridional transect in the northeastern Atlantic Ocean, J. Geophys. Res.-Oceans, 117, C04016, doi:10.1029/2011JC007137, 2012b. 842, 844, 845

Kirk, J.: Light and Photosynthesis in Aquatic Ecosystems, Cambridge University Press, 2011. 857

Levitus, S., Antonov, J., Boyer, T., and Stephens, C.: Warming of the world ocean, Science, 287, 2225–2229, doi:10.1126/science.287.5461.2225, 2000. 845

Liccardo, A., Fierro, A., Iudicone, D., Bouruet-Aubertot, P., and Dubroca, L.: Response of the deep chlorophyll maximum to fluctuations in vertical mixing intensity, Prog. Oceanogr., 109, 33–46, doi:10.1016/j.pocean.2012.09.004, 2013. 874

Losa, S. N., Kivman, G. A., and Ryabchenko, V. A.: Weak constraint parameter estimation for a simple ocean ecosystem model: what can we learn about the model and data?, J. Marine Syst., 45, 1–20, doi:10.1016/j.jmarsys.2003.08.005, 2004. 874

Lozier, M. S., Dave, A. C., Palter, J. B., Gerber, L. M., and Barber, R. T.: On the relationship between stratification and primary productivity in the North Atlantic, Geophys. Res. Lett., 38, L18609, doi:10.1029/2011GL049414, 2011. 841

Mahadevan, A., D'Asaro, E., Lee, C., and Perry, M. J.: Eddy-driven stratification initiates north atlantic spring phytoplankton blooms, Science, 337, 54–58, doi:10.1126/science.1218740, 2012. 846

Martin, S.: An introduction to Ocean Remote Sensing, ISBN 978-0-521-80280-2, Cambridge University Press, 2004. 865

Martinez, E., Antoine, D., D'Ortenzio, F., and Gentili, B.: Climate-driven basin-scale decadal oscillations of oceanic phytoplankton, Science, 326, 1253–1256, doi:10.1126/science.1177012, 2009. 840

McGillicuddy, D. J., Anderson, L. A., Bates, N. R., Bibby, T., Buesseler, K. O., Carlson, C. A., Davis, C. S., Ewart, C., Falkowski, P. G., Goldthwait, S. A., Hansell, D. A., Jenkins, W. J., Johnson, R., Kosnyrev, V. K., Ledwell, J. R., Li, Q. P., Siegel, D. A., and Steinberg, D. K.:

OSD
11, 839–893, 2014

Eddy/wind interactions stimulate extraordinary mid-ocean plankton blooms, Science, 316, 1021–1026, doi:10.1126/science.1136256, 2007. 842

Mellard, J. P., Yoshiyama, K., Litchman, E., and Klausmeier, C. A.: The vertical distribution of phytoplankton in stratified water columns, J. Theor. Biol., 269, 16–30, doi:10.1016/j.jtbi.2010.09.041, 2011. 874

Mobley, C. D.: Light and Water: Radiative Transfer in Natural Waters, Academic Press, San Diego, California, 1994. 857

Morel, A., Gentili, B., Claustre, H., Babin, M., Bricaud, A., Ras, J., and Tièche, F.: Optical properties of the "clearest" natural waters, Limnol. Oceanogr., 52, 217–229, 2007. 858

Omta, A. W., Llido, J., Garcon, V., Kooijman, S. A. L. M., and Dijkstra, H. A.: The interpretation of satellite chlorophyll observations: the case of the Mozambique Channel, Deep-Sea Res.-Pt. I, 56, 974–988, doi:10.1016/j.dsr.2009.01.011, 2009. 842, 846, 851

O'Reilly, J., Maritorena, S., O'Brien, M., Siegel, D., Toole, D., Menzies, D., Smith, R., Mueller, J., Mitchell, B., Kahru, M., Chavez, F., Strutton, P., Cota, G., Hooker, S., McClain, C. R., Carder, K., Müller-Karger, F., Harding, L., Magnuson, A., Phinney, D., Moore, G., Aiken, J., Arrigo, K., Letelier, R. M., and Culver, M.: SeaWiFS Postlaunch Calibration and Validation Analyses, Part 3, Vol. 11 of Nasa Tech. Memo., edited by: Hooker, S. B. and Firestone, E. R., Nasa Goddard Space Flight Center, 49 pp., 2000. 844

Osborn, T.: Oceanic fine structure, Geophys. Astro. Fluid, 3, 321–345, 1972. 844

Peters, F., Arin, L., Marrasé, C., Berdalet, E., and Sala, M.: Effects of small-scale turbulence on the growth of two diatoms of different size in a phosphorus-limited medium, J. Marine Syst., 61, 134–148, doi:10.1016/j.jmarsys.2005.11.012, 2006. 850

Roget, E., Lozovatsky, I., Sanchez, X., and Figueroa, M.: Microstructure measurements in natural waters: methodology and applications, Prog. Oceanogr., 70, 126–148, doi:10.1016/j.pocean.2006.07.003, 2006. 842

Ryabov, A., Rudolf, L., and Blasius, B.: Vertical distribution and composition of phytoplankton under the influence of an upper mixed layer, J. Theor. Biol., 263, 120–133, doi:10.1016/j.jtbi.2009.10.034, 2010. 843, 846, 847, 849, 850, 851, 874

Siegel, D. A., Maritorena, S., Nelson, N. B., and Behrenfeld, M. J.: Independence and interdependencies among global ocean color properties: reassessing the bio-optical assumption, J. Geophys. Res.-Oceans, 110, C07011, doi:10.1029/2004JC002527, 2005. 852, 857

OSD
11, 839–893, 2014

Suggett, D. J., Borowitzka, M. A., and Prasil, O.: Chlorophyll *a* Fluorescence in Aquatic Sciences: Methods and Applications Chlorophyll *a* Fluorescence in Aquatic Sciences: Methods and Applications, Vol. 1, Springer, 2011. 845

Thi, N. P., Huisman, J., and Sommeijer, B.: Simulation of three-dimensional phytoplankton dynamics: competition in light-limited environments, J. Comput. Appl. Math., 174, 57–77, doi:10.1016/j.cam.2004.03.023, 2005. 874

Valenti, D., Denaro, G., La Cognata, A., Spagnolo, B., Bonanno, A., Basilone, G., Mazzola, S., Zgozi, S., and Aronica, S.: Picophytoplankton dynamics in noisy marine environment, Acta Phys. Pol. B, 43, 1227–1240, doi:10.5506/APhysPolB.43.1227, 2012. 874

van de Poll, W. H., Kulk, G., Timmermans, K. R., Brussaard, C. P. D., van der Woerd, H. J., Kehoe, M. J., Mojica, K. D. A., Visser, R. J. W., Rozema, P. D., and Buma, A. G. J.: Phytoplankton chlorophyll *a* biomass, composition, and productivity along a temperature and stratification gradient in the northeast Atlantic Ocean, Biogeosciences, 10, 4227–4240, doi:10.5194/bg-10-4227-2013, 2013. 845, 849, 850, 854

Wernand, M. R., van der Woerd, H. J., and Gieskes, W. W. C.: Trends in ocean colour and chlorophyll concentration from 1889 to 2000, worldwide, Plos One, 8, e63766, doi:10.1371/journal.pone.0063766, 2013. 840

OSD
11, 839–893, 2014

Table 1. Standard values used in the PGM.

Symbol	Description	Units	Value
	System parameters		
Z_b	Depth of the system	m	200
I_{in}	Incident light intensity	µmol photons $m^{-2} s^{-1}$	390–625
N_b	Nutrient concentration at Z_b	mmol nutrients m^{-3}	5.7–12.7
K_{bg}	Background attenuation of sea water	m^{-1}	0.032
K_T	Vertical mixing coefficient (depth dependent)	$m^2 s^{-1}$	0.4×10^{-2}–1.2
	Biological parameters		
k	Absorption coefficient of phytoplankton	m^2 cell^{-1}	1.0×10^{-9}
μ_{max}	Maximum specific growth rate	h^{-1}	0.04
H_I	Half saturation constant of light limited growth	µmol photons $m^{-2} s^{-1}$	58–125
H_N	Half saturation constant of nutrient limited growth	mmol nutrients m^{-3}	0.5–3
m	Specific loss rate	h^{-1}	0.01
α	Nutrient content of phytoplankton	mmol nutrients cell^{-1}	1.0×10^{-9}
ε	Nutrient recycling coefficient	–	0.5
v	Sinking velocity	$m h^{-1}$	0.042
	Numerical parameters		
Δz	Spatial step	m	0.25
Δt	Temporal step	h	24

OSD
11, 839–893, 2014

Table 2. Value ranges used in other models. [a] Here the units were converted from $[\mathrm{mmol\,N}]^{-1}$ to $[\mathrm{cell}]^{-1}$ using conversion factor 1×10^{-9} mmol nutrients cell^{-1} by Ryabov et al. (2010). [b] In unit [mmol phosphorus m^{-3}].

Ref.	HI µmol photons m^{-2} s^{-1}	HN mmol nutrients m^{-3}	K_{bg} m^{-1}	k 10^{-10} m^2 cell^{-1}
Losa et al. (2004)	–	0.3	0.04	0.3[a]
Fiechter (2012)	–	1.0	0.067	0.4[a]
Huisman and Sommeijer (2002)	30	–	0.2	0.15
Valenti et al. (2012)	20	0.0425	0.045	6.0
Mellard et al. (2011)	50	0.032[b]	0.1	0.1
Thi et al. (2005)	10–20		0.2	0.15–0.3
Liccardo et al. (2013)	20	0.02	0.05	6.0
	10–50	0.02–1.0	0.04–0.2	0.15–6.0

OSD
11, 839–893, 2014

Table 3. Parameters and boundary conditions applied during the sensitivity analysis.

Station Description	Latitude	Cruise	N_b mmol nutrients m^{-3}	I_{in} µmol photons m^{-2} s^{-1}	H_N mmol nutrients m^{-3}	H_I µmol photons m^{-2} s^{-1}
Southern	40.5° N	Summer	5.7	625	0.5	58
Northern	60.7° N	Summer	12.7	390	2.5	80
Transition	45.5° N	Spring	8.8	530	3.0	125

OSD
11, 839–893, 2014

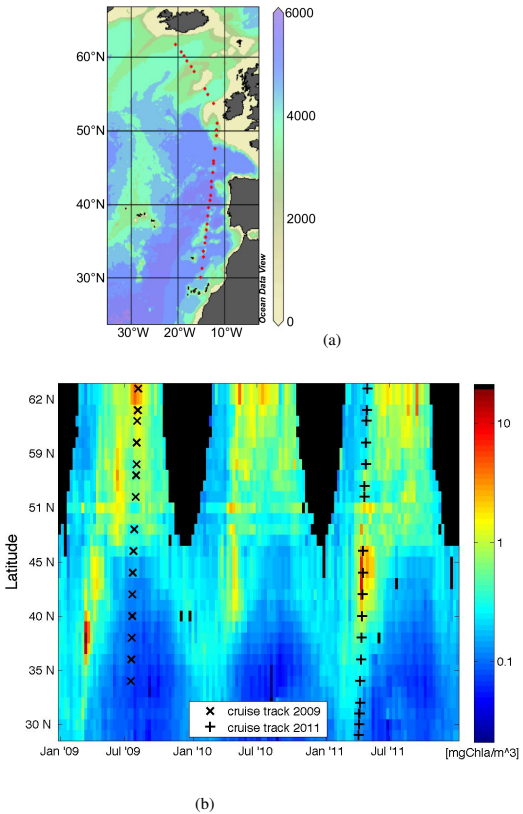

Fig. 1. (a) Bathymetry of the North Atlantic with the track of the STRATIPHYT cruises. The colors show the water depth in meters. **(b)** MODIS Aqua Chlorophyll *a* surface concentration plotted along the track in **(a)**. The black crosses and plusses indicate measurement stations during the STRATIPHYT cruises in summer 2009 and spring 2011, respectively.

OSD
11, 839–893, 2014

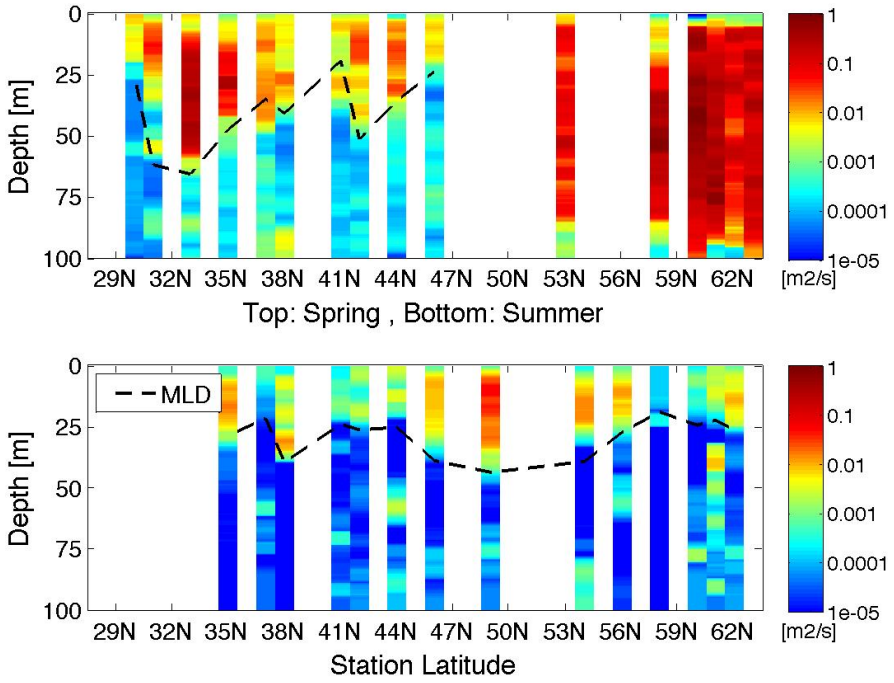

Fig. 2. Interpolated and smoothed vertical mixing coefficient in spring (top) and summer (bottom) along the transect in Fig. 1a. The dashed curve indicates the MLD.

OSD
11, 839–893, 2014

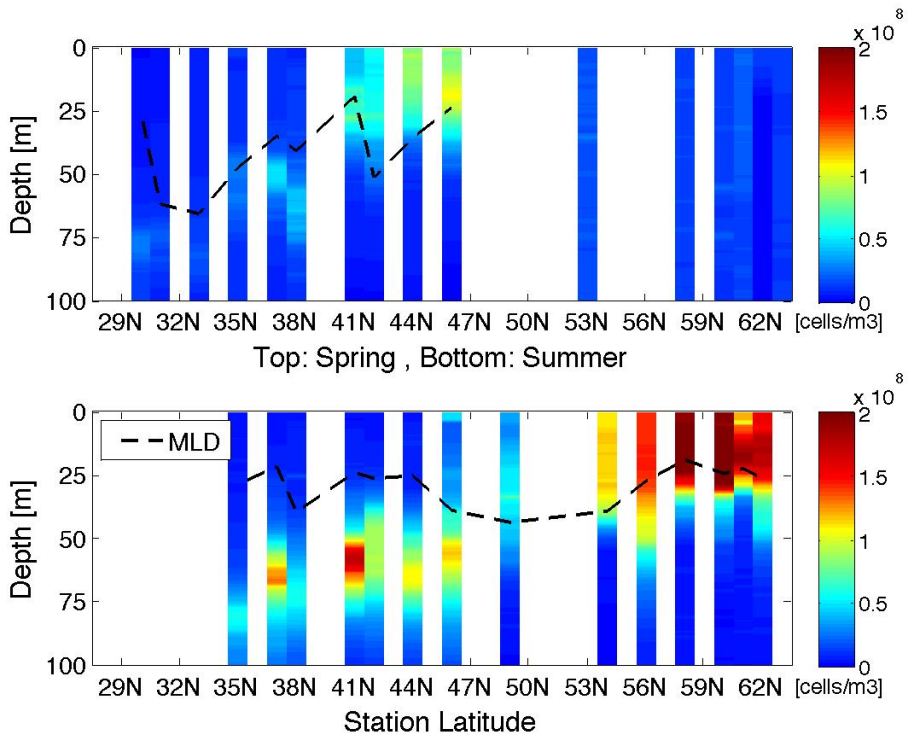

Fig. 3. Phytoplankton cell concentration converted from the interpolated and smoothed Fluorescence, Chelsea Aqua 3 Chl *a* concentrations measured during the spring (top) and summer (bottom) cruise. The dashed curve indicates the MLD.

OSD
11, 839–893, 2014

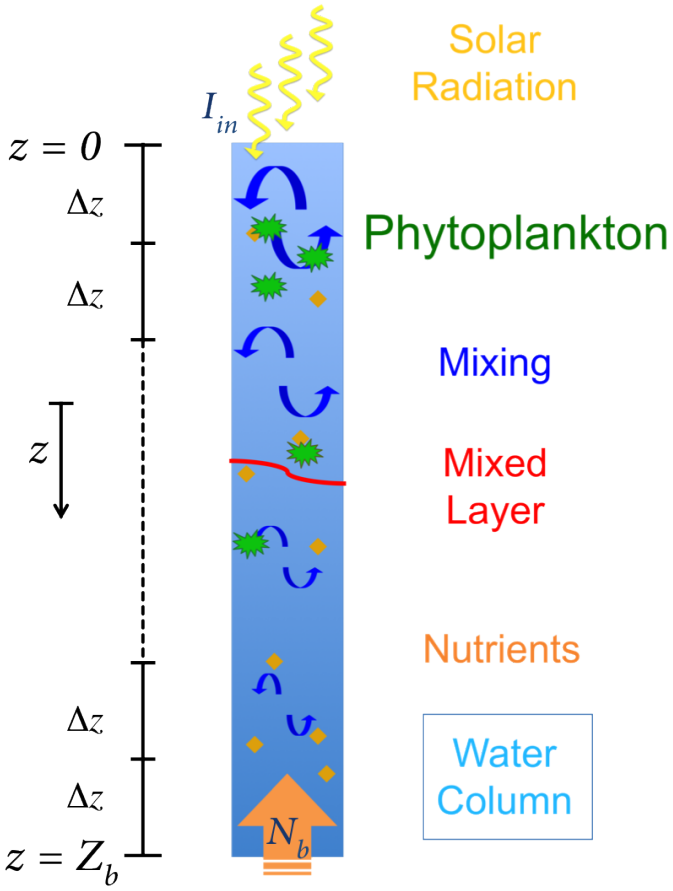

Fig. 4. Schematic representation of the processes and setup of the PGM.

OSD
11, 839–893, 2014

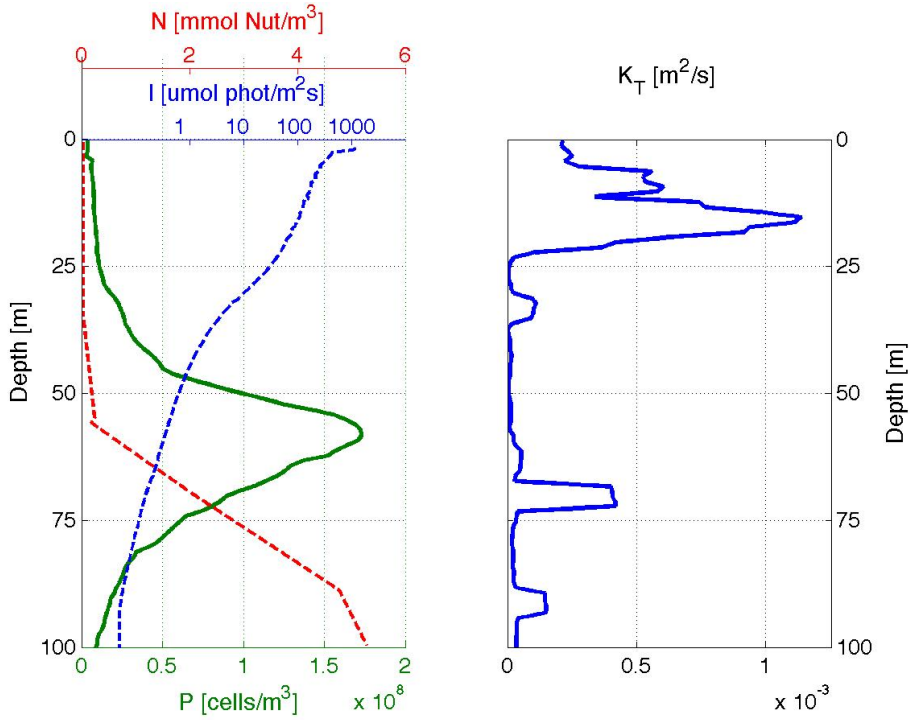

Fig. 5. Measurement data at (13.2° W, 40.5° N) on 23 July 2009. Left panel: phytoplankton concentration (green), nutrient density (sum of phosphate, nitrogen dioxide, and nitrate; red dashed), and light intensity (blue dashed). Right panel: vertical mixing coefficient K_T.

OSD
11, 839–893, 2014

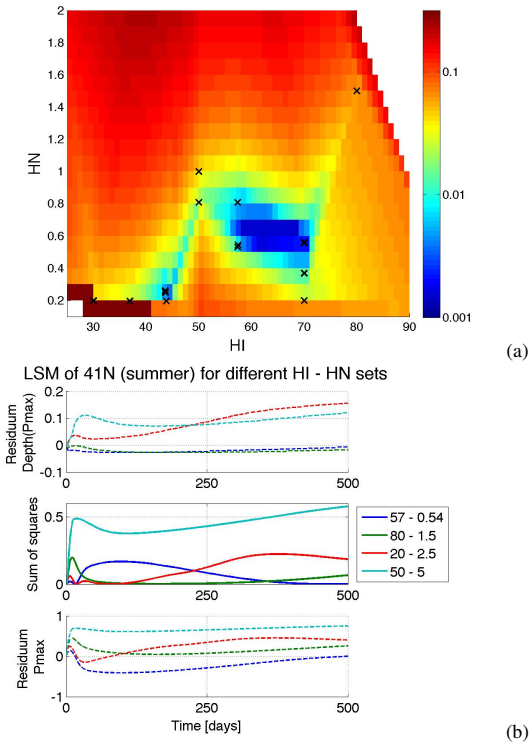

Fig. 6. (a) Map of the sum of squares S as a measure of proximity to the measured state for the southern station. The crosses indicate modelled data based on which the contour plot is generated. **(b)** The temporal evolution of (top) the residual defined by the depth of the maximum phytoplankton concentration, (center) the sum of squares *S* as a result of the two residuals, and (bottom) the residual defined by the value of the maximum phytoplankton concentration. A negative value for the residual indicates that the computed PGM value is too high with respect to observations.

OSD
11, 839–893, 2014

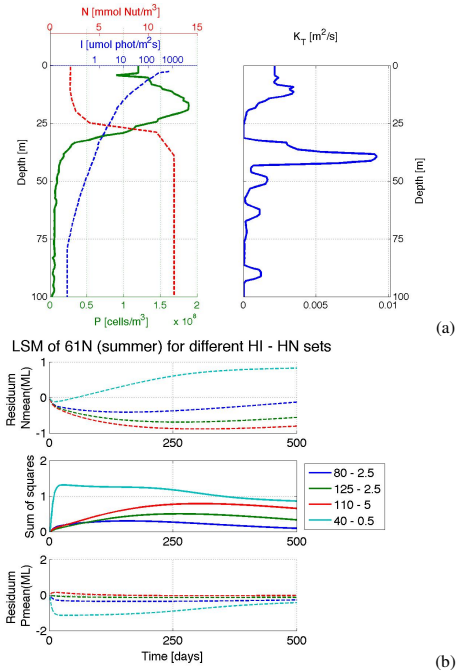

Fig. 7. (a) Measurements at (19.3° W, 60.7° N) on 6 August 2009. Left panel: phytoplankton concentration (green), nutrient density (red dashed), and light intensity (blue dashed). Right panel: vertical mixing coefficient K_T. **(b)** The temporal evolution of (top) the residual defined by the depth of the maximum phytoplankton concentration, (center) the sum of squares S as a result of the two residuals, and (bottom) the residual defined by the value of the maximum phytoplankton concentration. Negative values for the residuals indicate that the computed PGM value is too high compared to observations.

OSD
11, 839–893, 2014

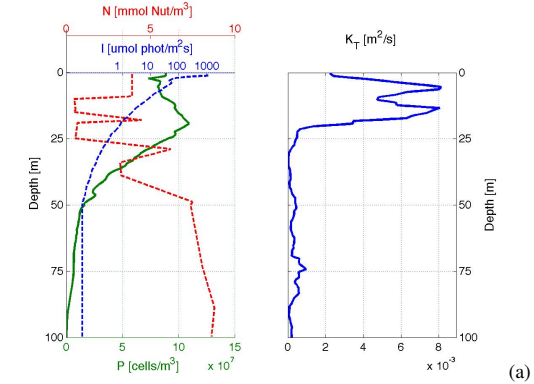

Fig. 8. (a) Measurements at (12.9° W, 45.5° N) on 21 April 2011. Left panel: phytoplankton concentration (green), nutrient density (red dashed), and light intensity (blue dashed). Right panel: vertical mixing coefficient K_T. **(b)** Temporal evolution of (top) the residual defined by the depth of the maximum phytoplankton concentration, (center) the sum of squares S as a result of the two residuals, and (bottom) the residual defined by the value of the maximum phytoplankton concentration. Negative values for the residuals indicate that the computed PGM value is too high compared to observations.

OSD
11, 839–893, 2014

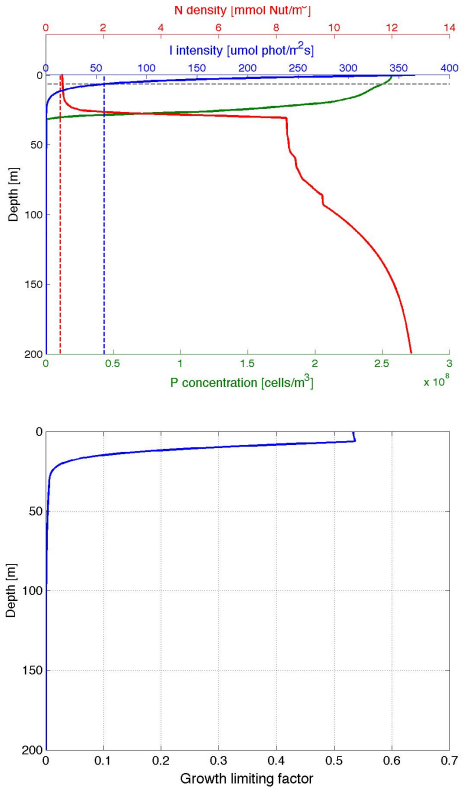

Fig. 9. Depth profile of the northern station with the half saturation constants determined by the LSM. **(a)** The phytoplankton concentration is given in green, light intensity as the solid blue line, and the nutrient concentration as the solid red line. H_I is indicated by the dashed blue line and H_N is indicated by the dashed red line. The dashed grey line gives the depth at which nutrient limited growth (at the surface) changes to light limited growth. **(b)** The resulting growth factor over depth as given by the minimum function on the left hand side of Eq. (7).

OSD
11, 839–893, 2014

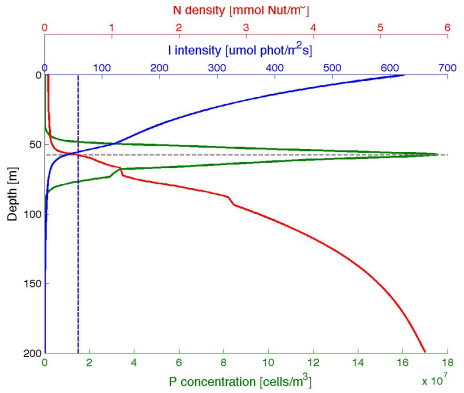

Fig. 10. Depth profile of the southern station with the half saturation constants determined by the LSM. **(a)** The phytoplankton concentration is given in green, light intensity in the solid blue line, and the nutrient concentration as the solid red line. H_I is indicated by the dashed blue line and H_N is indicated by the dashed red line (coincides with the dashed blue line). The dashed grey line gives the depth at which nutrient limited growth (at the surface) changes to light limited growth. **(b)** The resulting growth factor over depth as given by the minimum function on left hand side of Eq. (7).

OSD
11, 839–893, 2014

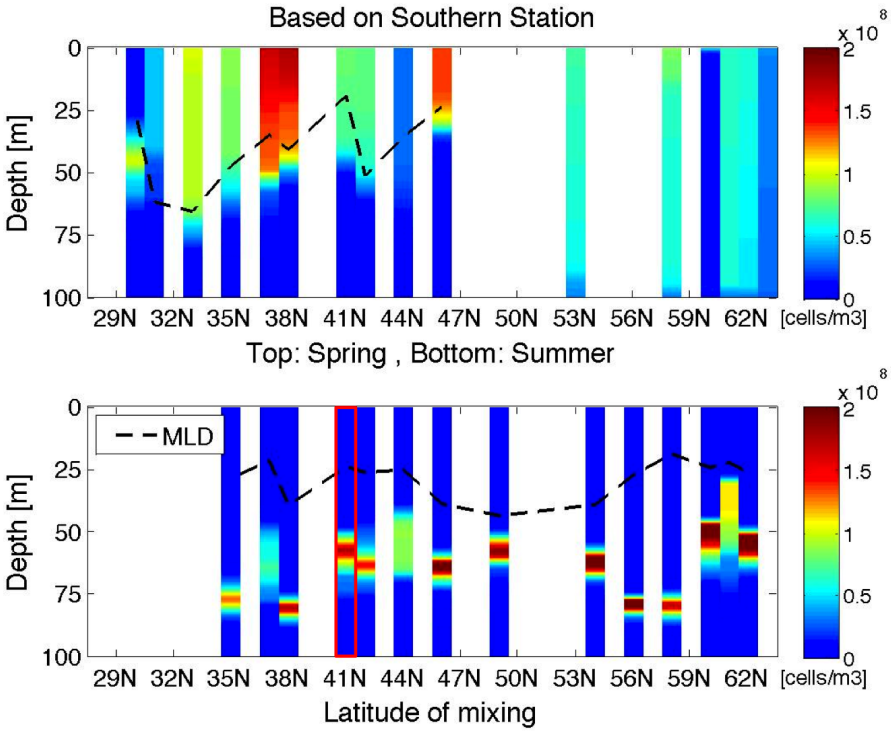

Fig. 11. Model results based on the southern station with vertical mixing profiles of the spring cruise (top) and summer cruise (bottom). The red box marks the reference station.

OSD
11, 839–893, 2014

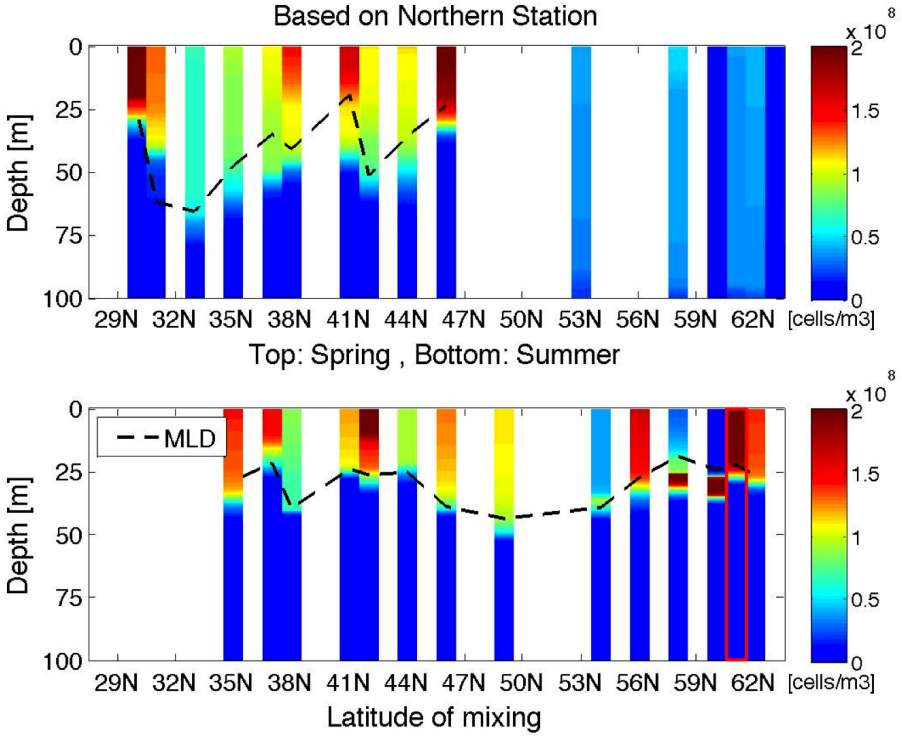

Fig. 12. Model results based on the southern station with vertical mixing profiles of the spring cruise (top) and summer cruise (bottom).The red box marks the reference station.

OSD
11, 839–893, 2014

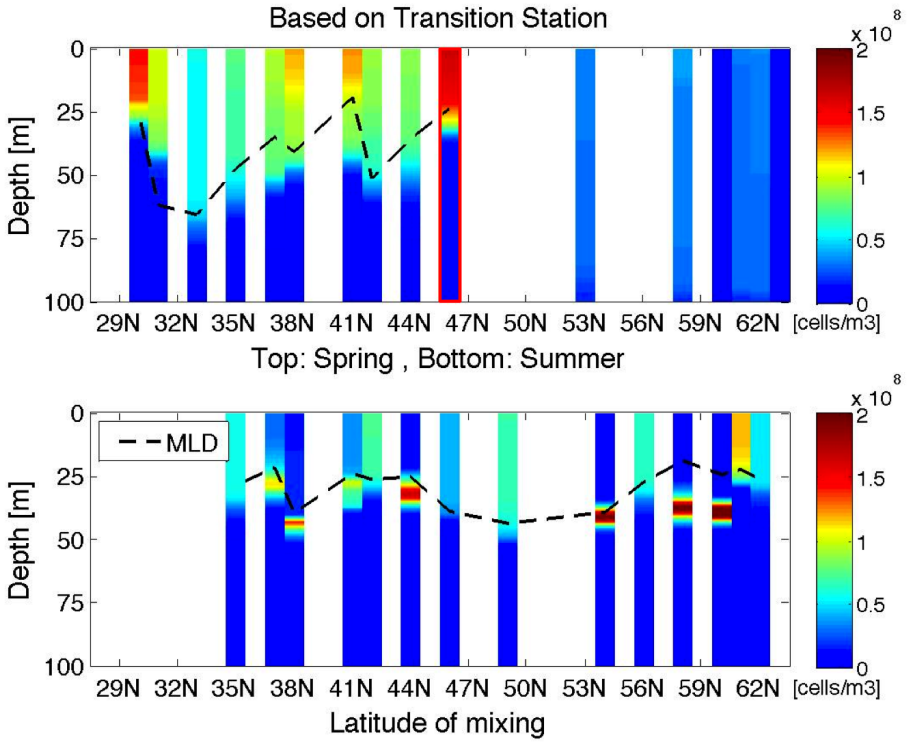

Fig. 13. Model results based on the southern station with vertical mixing profiles of the spring cruise (top) and summer cruise (bottom). The red box marks the reference station.

OSD
11, 839–893, 2014

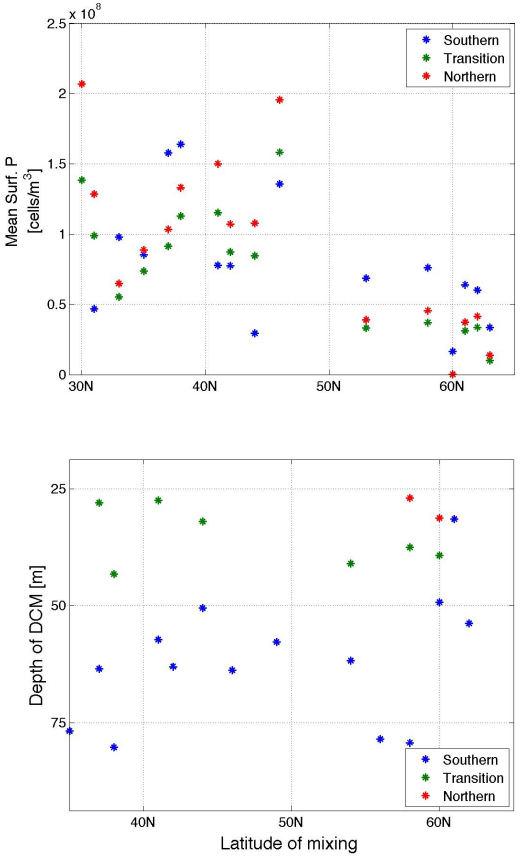

Fig. 14. Comparison of the PGM results for the three reference stations. **(a)** Mean surface phytoplankton concentration based on the spring vertical mixing profiles. **(b)** Depth of the DCM based on the summer vertical mixing profiles.

OSD
11, 839–893, 2014

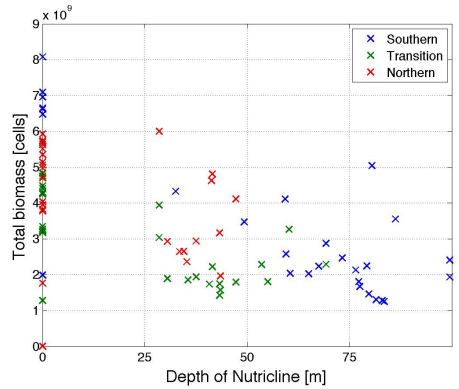

Fig. 15. (a) The total biomass integrated over the water column as a function of the depth of the nutricline. **(b)** Normalised surface phytoplankton concentration vs. the relative nutrient flux for the three reference stations and with the spring and summer vertical mixing profiles applied in the PGM. Only nutrient limited states are taken into account.

OSD
11, 839–893, 2014

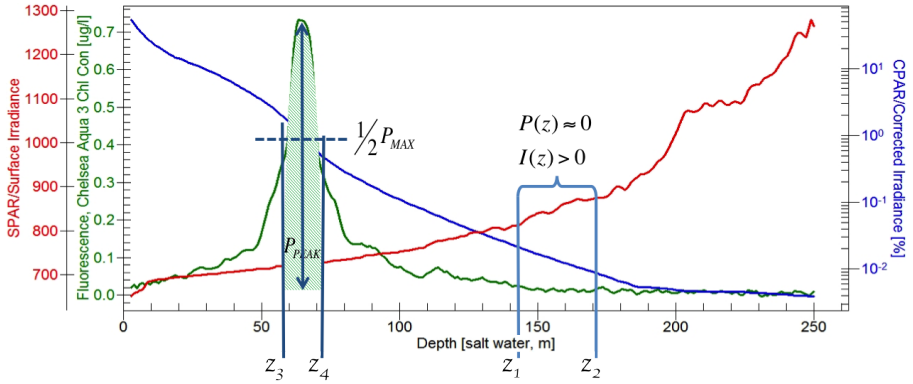

Fig. A1. CTD data at Station 7 (36.3° N, 13.5° W) 21 July 2009, 11 a.m. Depth profile of the Chl *a* concentration (green line), depth profile of the corrected irradiance (blue line), and surface irradiance at time of measured depth (red line). In light blue the depth section used to extract K_{bg} is sketched. The green-shaded area symbolises the phytoplankton concentration which is used to determine k.

OSD
11, 839–893, 2014

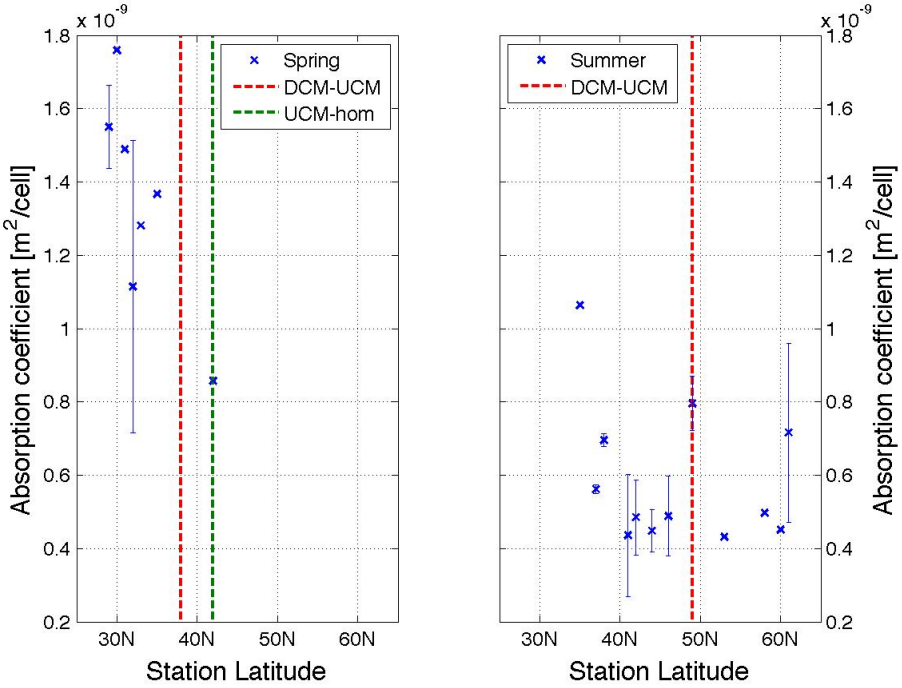

Fig. A2. *k* based on light intensity profiles and Chl *a* concentration profiles measured in spring (left) and summer (right), respectively. The vertical lines define the latitude at which the system changes its state, while red is the transition from a DCM to a UCM state and green from a UCM to a homogeneously mixed state.

OSD
11, 839–893, 2014

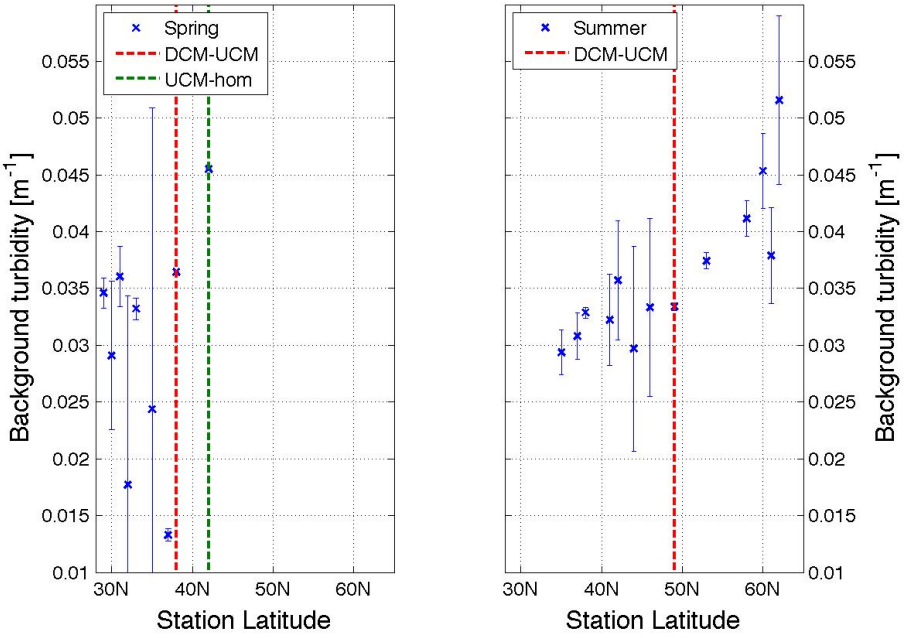

Fig. A3. K_{bg} based on light intensity profiles measured in spring (left) and summer (right), respectively. The vertical dashed lines define the latitude at which the system changes its state, where red is the transition from a DCM to a UCM state and green from a UCM to a homogeneously mixed state.

OSD
11, 839–893, 2014